Chapter 14
FRP-RC Slabs Under Punching Shear: Assessment of Existing Models

Maged Tawfik, Taha Ibrahim, Mahmood Ahmad, Ahmed F. Deifalla, Ahmed Awad, and Amr El-Said

Abstract The purpose of this study is to examine the punching shear behavior of concrete slabs reinforced with FRP. We compared and quickly described 21 strength models. In addition, based on overall performance, strength models were contrasted with one another in terms of the experimentally observed strength. Conclusions were made and discussed, which may help future design codes evolve more effectively, It was decided where to focus future studies. This might aid in the development of future design codes. The ACI is the least realize model, although taking into account the effects of size, dowel action, depth-to-control perimeter ratio, concrete compressive strength, and shear span-to-depth ratio.

Keywords Design · Punching shear · GFRP · CFRP · FRP · BFRP

M. Tawfik · A. El-Said
Department of Civil Engineering, The Higher Institute of Engineering, El Shrouk, Cairo, Egypt
e-mail: m.nashaat@sha.edu.eg

A. El-Said
e-mail: a.elsayed@sha.edu.eg

T. Ibrahim
Benha University in Egypt, Banha, Egypt
e-mail: taha.ibrahim@feng.bu.edu.eg

M. Ahmad
University of Engineering and Technology Peshawar, Peshawar, Pakistan
e-mail: ahmadm@uetpeshawar.edu.pk

A. F. Deifalla (✉)
Future University in Egypt, New Cairo, Egypt
e-mail: Ahmed.deifalla@fue.edu.eg

A. Awad
Faculty of Engineering, October University for Modern Sciences and Arts, Giza, Egypt

A. S. Mosallam et al. (eds.), *Advances in Smart Materials and Innovative Buildings Construction Systems*, Sustainable Civil Infrastructures,
https://doi.org/10.1007/978-3-031-47428-6_14

14.1 Introduction

Figure 14.1 depicts the victims of a parking garage collapse in 2021 that happened unexpectedly on a playground in Spain. Additionally, much of the reinforced concrete (RC) slab Punching shear design is empirical or semi-empirical. As a result, extensive research is being conducted to better understand the punching shear. However, the process of the slabs' punching shear is intricate, making further research into it necessary (Deifalla 2020, 2021a, b; FIB 2007). The following list of resistance mechanisms makes up the punching shear resistance of concrete slabs lacking shear reinforcements: Flexural reinforcements, aggregate, and uncracked concrete are resisting the shear in different ways. Flexural reinforcements resist the shear by dowels shear, aggregate resist the shear across the sides of diagonal concrete cracks through the aggregate interlock, and uncracked concrete resists the shear through direct shear (Yooprasertchai et al. 2021a, b; Wu et al. 2022; Bywalski et al. 2020).

Fiber-reinforced polymer (FRP) reinforcements are frequently used in place of traditional reinforcement in concrete slabs to prevent corrosion issues (Ebid and Deifalla 2021). FRP reinforcements also offer a good strength-to-weight ratio and are magnetically neutral. As a result, it is the greatest option for structures exposed to harsh weather factors, including freeze thaw cycles, deicing salts, and wet dry cycles. Numerous researchers have examined, mostly through experimental studies, the behavior of brand-new and preexisting beams and slabs reinforced with FRP bars or textiles under one-way and punching shear as well as torsion (Ali et al. 2021; Hassan and Deifalla 2015; Deifalla 2015; Deifalla et al. 2014, 2015). Punching

Fig. 14.1 Parking garage atop a playground collapsed (Deifalla 2022)

shearing of concrete FRP reinforcements was the subject of several research projects, but very few mechanical models were created for this situation (Wu et al. 2022). Because the FRP failure is brittle, the fissures in FRP-reinforced concrete are larger before failure than in traditional RC (Elmeligy et al. 2017; Failed 2021), or (Deifalla et al. 2021). Wider fractures have a considerable impact on the different punching shear strength processes.

The early 1960s ideas served as the foundation for the conventional punching shear design formulae for RC slabs. These models were based on time tested specimens, but extensive testing over the last few decades has shown various flaws in this approach, including, and not limited to the effect of size and the models' extreme lack of conservatism in many circumstances (Shen et al. 2022). Because of this, there is opportunity for advancements in the punching shear design models, which could aid in design code development (Kuchma et al. 2019; Collins 2001).

In this work, the punching shear strength of concrete slabs reinforced with FRP will be evaluated using the methods currently in use. The punching shear strength of FRP-reinforced concrete slabs was reviewed using the most recent design regulations, manuals, and models. A detailed analysis of slabs made of FRP reinforced concrete that were subjected to two way load during experimental testing. The strength estimated using each model is contrasted with the strength determined through testing. There was a discussion and sketch of the closing comments.

14.2 Simplified Strength Models

Several streamlined strength models have been put up for the Punching shear strength of FRP and RC slabs, either via adaptations for ordinary concrete slabs or empirical based on scant tested data. The North American design codes' punching shear design requirements ignored the impact of flexure reinforcement on strength. They concentrated on the compression zone's direct shear resistance. This could make sense for traditional steel reinforcements that are substantially stiffer than FRP ones. Therefore, the Punching shear strength is governed by the direct shear component. Dowel motion, however, could be a bigger contributor to the strength because the FRP is substantially less rigid than the steel one. In this section, many models' specifics and histories are detailed.

V is the failure load for punching shears. E Is the modulus of elasticity for FRP. Effective depth is d. Compressive strength of concrete is $f_c^{'}$. The dimensions of the slab are A and B, the dimensions of column are c, b, and the ratio of flexure reinforcement is ρ. The modulus of elasticity of the steel is E_s. The control perimeter at 0. $5d$, denoted as $b_{0.5d}$, is equal to $2(b + c + 2d)$. The control perimeter at 1. $5d$, denoted as $b_{1.5d}$, is equal to $2(b + c + 6d)$. The control perimeter at $b_{2.0d}$, denoted by the symbol $2.0d$, is equal to $2(b + c + 8d)$.

The models included the following: Gardner (1990), JSCE (1997), El-Ghandour et al. (2003); Mattys and Taerwe (2000), Ospina et al. (2003), Zaghloul and Razaqpur (2003), Jacbson et al. (2005), ACI (2015), El-Gamal et al. (2005); Zhang (2006a, b);

Theodorkopoulos and Swamy (2007), CSA-S806-12 (2012), Nguyen and Rovnak (2013), Hassan et al. (2017), Kara and Sinani (2017), Oller et al. (2018), CCCM (Kara and Sinani 2017), Hemzah et al. (2019), El-Gendy and El-Salakawy (2020), Ju et al. (2021), Alrudaini (2022).

Table 14.1 compares the different design models, and it is evident that there is no consensus among researchers on the factors that should be considered and the approach to do so. The impact of compressive strength of concrete in terms of $\left(f_c^{'}\right)^{1/3}$ or $\left(f_c^{'}\right)^{1/2}$ was considered in all design methodologies. For flexure reinforcement, the majority of systems used a dowel action.

It was seen as $(\rho)^{1/3}$ or $(\rho)^{1/2}$. In terms of modulus of elasticity, which was regarded as $(E)^{1/3}$, or $(E)^{1/2}$. More than half of the approaches contained the FRP type. In terms of the size effect, almost half the ways $(1/d)^{1/4}$, $(1/d)^{1/5}$, $(1/d)^{1/2}$, or $\frac{2}{\sqrt{1+d/200}}$. included the ratio of $(0.44 + 20.8d/b_{0.5d})$, $(1 + 8d/b_{0.5d})$, $(0.19 + 4d/b_{0.5d})$, $(0.65 + 4d/b_{0.5d})$, $(1 + 8d/b_{0.5d})$, $(0.65 + 4d/b_{0.5d})$, $(d/b_{0.5d})^{1/2}$, or $(d/b_{0.5d})^{1/5}$. between the critical perimeter and depth, the compression zone and the shear span to depth ratio were two highly restricted models.

14.3 Tested Database Profile

Punching shear has caused a considerable number of experimentally tested specimens to fail during the past 30 years. the largest experimental database in comparison to earlier research (Deifalla 2022; Marí et al. 2015; El-Gendy and El-Salakawy 2020; Alrudaini 2022). 248 slabs reinforcement with FRP in all were gathered from 50 distinct research trials. All the grouping slabs were loaded with punching shear, and they all abruptly failed. The database's specifics are covered in other publications. Although FRP reinforcements can take various forms and arrangements, these differences were considered in terms of ρ and E. All variables are regularly distributed and have a large range of values. Table 14.2 shows RC slabs with FRP reinforcements under two way shear loads for experimental database. The tested column and slab connections' frequencies and ranges when using FRP is shown Fig. 14.2.

14.4 Evaluation of Chosen Models

The strength of the slab-column connection in the experimental data base was calculated using all the gathered models. The terms are graphical, statistical goodness, and central tendency of fit were used to define three areas of comparison. The safety ratio (SR) was determined as the difference between the measured and calculated strengths. A SR value that is almost one indicates that the estimate is correct. A SR

Table 14.1 Comparisons between designed models

Model designed	Location of critical perimeter	Effect of size	Dowel action	Modulus of elasticity	Strength of concrete
G	$1.5d$	$(d)^{-1/4}$	$(\rho)^{1/3}$	–	$\left(f_c^{'}\right)^{1/3}$
JSCE	$0.5d$	$(d)^{-1/4}$	$(\rho)^{1/3}$	$(E)^{1/3}$	$\left(f_c^{'}\right)^{1/2}$
Gd	$1.5d$	$(d)^{-1/4}$	$(\rho)^{1/3}$	$(E)^{1/3}$	$\left(f_c^{'}\right)^{1/3}$
MT	$1.5d$	$(d)^{-1/4}$	$(\rho)^{1/3}$	$(E)^{1/3}$	$\left(f_c^{'}\right)^{1/3}$
O	$1.5d$	–	$(\rho)^{1/3}$	$(E)^{1/2}$	$\left(f_c^{'}\right)^{1/3}$
Z	$0.5d$	–	$(\rho)^{1/3}$	$(E)^{1/3}$	$\left(f_c^{'}\right)^{1/3}$
Jb	$1.5d$	$(d)^{-1/4}$	$(\rho)^{1/2}$	–	$\left(f_c^{'}\right)^{1/2}$
ACI	$0.5d$	–	–	–	$\left(f_c^{'}\right)^{1/2}$
EG	$0.5d$	–	$(\rho)^{1/3}$	$(E)^{1/3}$	$\left(f_c^{'}\right)^{1/2}$
Zg	$1.5d$	$(d)^{-1/5}$	$(\rho)^{1/2}$	$(E)^{1/2}$	$\left(f_c^{'}\right)^{1/3}$
TS	$0.5d$	$(d)^{-1/6}$	–	–	$\left(f_c^{'}\right)^{2/3}$
CSA	$0.5d$	–	$(\rho)^{1/3}$	$(E)^{1/3}$	$\left(f_c^{'}\right)^{1/3}$
NR	$0.5d$	$(d)^{-1/2}$	$(\rho)^{1/3}$	$(E)^{1/3}$	$\left(f_c^{'}\right)^{1/3}$
H	$0.5d$	$(d)^{-1/6}$	$(\rho)^{1/3}$	$(E)^{1/3}$	$\left(f_c^{'}\right)^{1/3}$
KS	$1.5d$	–	$(\rho)^{1/3}$	$(E)^{1/3}$	$\left(f_c^{'}\right)^{1/3}$
CCCM	$0.5d$	$2/\sqrt{1+d/200}$	$(\rho)^{1/3}$	$(E)^{1/3}$	$\left(f_c^{'}\right)^{2/3}$
Hz	$0.5d$	–	$(\rho)^{0.39}$	$(E)^{0;3}$	$\left(f_c^{'}\right)^{1/6}$
EE-(a)	$0.5d$	–	$(\rho)^{1/3}$	$(E)^{1/3}$	$\left(f_c^{'}\right)^{1/2}$
EE-(b)	$0.5d$	$(d)^{-1/6}$	$(\rho)^{1/3}$	$(E)^{1/3}$	$\left(f_c^{'}\right)^{1/3}$
Ju	$0.5d$	–	$(\rho)^{1/2}$	$(E)^{1/2}$	$\left(f_c^{'}\right)^{1/2}$
A	$0.5d$	–	$(\rho)^{1/3}$	$(E)^{1/3}$	$\left(\mathrm{f_c^{'}}\right)^{1/3}$

Table 14.2 Experimental database of shear loads under two way on RC slabs with FRP reinforcements

Spec. title	References	Failure load (kN)	Modulus of elasticity (GPa)	FRP Type	Rft ratio	Cylindrical comp. strength (MPa)	Width of column (mm)	Length of column (mm)	Depth of slab (mm)	Width of slab (mm)	Length of slab (mm)
CFRC,SN1	Ahmad et al. (1993)	93	113	CFRP	0.95	42.3	75	75	60	690	690
CFRC,SN2		78	113	CFRP	0.95	44.5	75	75	60	690	690
CFRC,SN3		96	113	CFRP	0.95	39	100	100	60	690	690
CFRC,SN4		99	113	CFRP	0.95	36.5	100	100	60	690	690
1	Banthia et al. (1995)	65	100	CFRP	0.3	41	100	100	55	600	600
2		61	100	CFRP	0.3	53	100	100	55	600	600
3		72	100	CFRP	0.3	41.7	100	100	55	600	600
1	Bank and Xi (1995)	186	143	CFRP	2.1	30	250	250	75	1500	1800
2		179	143	CFRP	2.1	30	250	250	75	1500	1800
3		199	143	CFRP	1.8	30	250	250	75	1500	1800
4		198	156	CFRP	2.1	30	250	250	75	1500	1800
5		201	156	CFRP	1.8	30	250	250	75	1500	1800
6		190	156	CFRP	1.5	30	250	250	75	1500	1800
1	Louka (1999)	500	41.3	GFRP	1	45	575	225	175	1800	3000
2		1050	41.3	GFRP	1	45	575	225	175	1800	3000
3		875	39.3	GFRP	1	45	575	225	175	1800	3000
4		1090	39.3	GFRP	1	45	575	225	175	1800	3000
5		1180	39.3	GFRP	1	45	575	225	175	1800	3000
C1		1000	100	CFRP	1	55	575	225	175	1800	3000

(continued)

Table 14.2 (continued)

Spec. title	References	Failure load (kN)	Modulus of elasticity (GPa)	FRP Type	Rft ratio	Cylindrical comp. strength (MPa)	Width of column (mm)	Length of column (mm)	Depth of slab (mm)	Width of slab (mm)	Length of slab (mm)
C2		1200	100	CFRP	1	55	575	225	175	1800	3000
C3		1328	100	CFRP	1	55	575	225	175	1800	3000
H2		1055	160	Hybrid	1	45	575	225	175	1800	3000
H4		1096	160	Hybrid	1	45	575	225	175	1800	3000
H5		1183	160	Hybrid	1	45	575	225	175	1800	3000
C1	Ospina et al. (2003)	181	91.8	CFRP	0.25	37	150	150	95	1000	1000
C1'		189	91.8	CFRP	0.25	35.8	230	230	95	1000	1000
C2		255	95	CFRP	1.05	36.5	150	150	95	1000	1000
C2'		273	95	CFRP	1.05	36.5	230	230	95	1000	1000
C3		347	92	CFRP	0.55	33.5	150	150	125	1000	1000
C3'		343	92	CFRP	0.55	34.2	230	230	125	1000	1000
CS		142	148	CFRP	0.2	32.5	150	150	95	1000	1000
CS'		150	148	CFRP	0.2	33.3	230	230	95	1000	1000
H1		207	37.3	HFRP	0.65	35.7	150	150	95	1000	1000
H2		231	40.7	HFRP	3.75	35.7	150	150	90	1000	1000
H2'		171	40.7	HFRP	3.75	35.7	80	80	90	1000	1000
H3		237	44.8	HFRP	1.25	32	150	150	120	1000	1000
H3'		217	44.8	HFRP	1.25	32	80	80	120	1000	1000
1	Rahman et al. (2000)	622	85	GFRP	0.3	42	250	150	160	2500	2000
2		698	85	GFRP	0.3	42	250	150	160	2500	2000

(continued)

Table 14.2 (continued)

Spec. title	References	Failure load (kN)	Modulus of elasticity (GPa)	FRP Type	Rft ratio	Cylindrical comp. strength (MPa)	Width of column (mm)	Length of column (mm)	Depth of slab (mm)	Width of slab (mm)	Length of slab (mm)
3		575	85	GFRP	0.3	42	250	150	160	2500	2000
4		534	85	GFRP	0.3	42	250	150	160	2500	2000
5		584	85	GFRP	0.3	42	250	150	160	2500	2000
1	Hassan et al. (2000)	1000	147	CFRP	0.58	59	575	225	165	3000	1800
2		1200	147	CFRP	0.58	59	575	225	165	3000	1800
3		1328	147	CFRP	0.58	59	575	225	165	3000	1800
1	Khanna et al. (2000)	756	42	GFRP	2.5	35	500	250	145	4000	2000
SG1	Matthys and Taerwe (2000)	170	45	GFRP	0.25	33.5	200	200	145	2000	2000
SC1		229	110	CFRP	0.2	34.8	200	200	145	2000	2000
SG2		271	45	GFRP	0.48	46.5	200	200	145	2000	2000
SG3		237	45	GFRP	0.48	30	200	200	145	2000	2000
SC2		317	110	CFRP	0.45	29.7	200	200	145	2000	2000
GFR-1	Zaghloul and Razaqpur (2003)	217	34	GFRP	0.75	29.7	250	250	120	2150	2150
GFR-2		260	34	GFRP	1.45	29.7	250	250	120	2150	2150
NEF-1		206	28.4	GFRP	0.88	37.5	250	250	120	2150	2150
ZJF5	Jacobson et al. (2005)	234	100	CFRP-	1	45	250	250	75	1760	1760

(continued)

Table 14.2 (continued)

Spec. title	References	Failure load (kN)	Modulus of elasticity (GPa)	FRP Type	Rft ratio	Cylindrical comp. strength (MPa)	Width of column (mm)	Length of column (mm)	Depth of slab (mm)	Width of slab (mm)	Length of slab (mm)
G-S1	Hussein et al. (2004)	249	42	GFRP	1.2	40	250	250	100	1830	1830
G-S2		218	42	GFRP	1.05	35	250	250	100	1830	1830
G-S3		240	42	GFRP	1.65	29	250	250	100	1830	1830
G-S4		210	42	GFRP	0.95	26	250	250	100	1830	1830
1	ACI (2015)	537	33	GFRP	0.95	27.5	635	250	175	2000	2300
2		536	33	GFRP	0.95	27.5	635	250	175	2000	2300
3		531	33	GFRP	0.95	27.5	635	250	175	2000	2300
7		721	33	GFRP	0.95	27.5	635	250	175	2000	2000
8		897	33	GFRP	0.95	27.5	635	250	175	2000	2000
G-S1	Zhang (2006a)	740	44.6	GFRP	1	49.5	600	250	160	2500	3000
G-S2		712	38.5	GFRP	2	44.2	600	250	160	2500	3000
G-S3		732	46.5	GFRP	1.2	49.2	600	250	160	2500	3000
C-S1		674	122.5	CFRP	0.35	49.5	600	250	165	2500	3000
C-S2		799	122.5	CFRP	0.7	44.5	600	250	165	2500	3000
GS2	Zhang et al. (2005)	218	42	GFRP	1.05	35	250	250	100	1830	1830
GSHS		275	42	GFRP	1.2	71	250	250	100	1830	1830

(continued)

Table 14.2 (continued)

Spec. title	References	Failure load (kN)	Modulus of elasticity (GPa)	FRP Type	Rft ratio	Cylindrical comp. strength (MPa)	Width of column (mm)	Length of column (mm)	Depth of slab (mm)	Width of slab (mm)	Length of slab (mm)
CS1	Zhang (2006b)	251	120	CFRP	0.4	31	250	250	100	1900	1900
CS2		293	120	CFRP	0.55	33	250	250	100	1900	1900
CS3		285	120	CFRP	0.75	25.5	250	250	100	1900	1900
CSHD1		325	120	CFRP	0.55	36	250	250	100	1900	1900
CSHD2		360	120	CFRP	0.75	38.5	250	250	100	1900	1900
CSHS1		399	120	CFRP	0.35	85.6	250	250	150	1900	1900
CHSHS2		446	120	CFRP	0.5	98.5	250	250	150	1900	1900
1	Tom (2007)	282	41	GFRP	1	70	250	250	110	1900	1900
2		319	41	GFRP	1.2	70	250	250	110	1900	1900
3		384	41	GFRP	1.5	70	250	250	110	1900	1900
4		589	41	GFRP	1.2	70	250	250	160	1900	1900
5		487	41	GFRP	1.2	70	250	250	145	1900	1900
6		437	41	GFRP	1.2	70	250	250	135	1900	1900
ZJEF1	Zaghloul (2007)	188	100	CFRP	1.35	25	250	250	120	1000	1760
ZJEF2		156	100	CFRP	0.95	27	250	250	120	1000	1760
ZJEF3		211	100	CFRP	1.38	55	250	250	120	1000	1760

(continued)

Table 14.2 (continued)

Spec. title	References	Failure load (kN)	Modulus of elasticity (GPa)	FRP Type	Rft ratio	Cylindrical comp. strength (MPa)	Width of column (mm)	Length of column (mm)	Depth of slab (mm)	Width of slab (mm)	Length of slab (mm)
ZJEF5		97	100	CFRP	1.38	28	250	250	80	1000	1760
ZJEF7		196	100	CFRP	1.38	26	450	250	120	1000	1760
ZJF8		178	100	CFRP	1.48	28	350	250	100	1760	1760
ZJF9		272	100	CFRP	1.48	57.5	250	250	100	1760	1760
G-S4	El-Gamal et al. (2007)	707	44.5	GFRP	1.2	44	600	250	155	2500	3000
G-S5		735	44.5	GFRP	1.2	44	600	250	155	2500	3000
F1	Zaghloul et al. (2008)	165	46	GFRP	1.1	37.5	200	200	80	1200	1200
F2		170	46	GFRP	0.8	33	200	200	110	1200	1200
F3		210	46	GFRP	1.3	38.5	200	200	80	1200	1200
F4		230	46	GFRP	1.55	39.5	200	200	80	1200	1200
GFU1	Lee et al. (2009)	222	48.2	GFRP	1.18	36.5	225	225	110	2300	2300
GFB2		246	48.2	GFRP	2.15	36.5	225	225	110	2300	2300
GFB3		248	48.2	GFRP	3	36.5	225	225	110	2300	2300
GFBF3		330	48.2	GFRP	3	33.9	225	225	110	2300	2300
S3	Zhu et al. (2010)	145	100	BFRP	0.3	33.5	150	150	135	1500	1500
S4		275	100	BFRP	0.55	35.5	150	150	135	1500	1500

(continued)

Table 14.2 (continued)

Spec. title	References	Failure load (kN)	Modulus of elasticity (GPa)	FRP Type	Rft ratio	Cylindrical comp. strength (MPa)	Width of column (mm)	Length of column (mm)	Depth of slab (mm)	Width of slab (mm)	Length of slab (mm)
S5		235	100	BFRP	0.45	32.9	150	150	135	1500	1500
S6		225	100	BFRP	0.45	32.5	150	150	135	1500	1500
S7		170	100	BFRP	0.45	22.5	150	150	135	1500	1500
S8		235	100	BFRP	0.45	41.8	150	150	135	1500	1500
S9		200	100	BFRP	0.45	40.6	150	150	135	1500	1500
NC-G-45	Min et al. (2010)	44	76	GFRP	0.78	48	25	25	45	300	300
NC-G-0/90		45	76	GFRP	0.78	48	25	25	45	300	300
NC-C-45		39	230	CFRP	0.25	48	25	25	45	300	300
NC-C-0/90		45	230	CFRP	0.25	48	25	25	45	300	300
SFRC-C-45		63	230	CFRP	0.25	48	25	25	45	300	300
UHPC-C-45		97	230	CFRP	0.25	180	25	25	45	300	300
UHPC-C-0/90		98	230	CFRP	0.25	180	25	25	45	300	300
A	Xiao (2010)	176	45.6	GFRP	0.42	22.2	150	150	130	1500	1500
B-2		209	45.6	GFRP	0.42	32.5	150	150	130	1500	1500
B-3		245	45.6	GFRP	0.55	32.5	150	150	130	1500	1500
B-4		167	45.6	GFRP	0.3	32.5	150	150	130	1500	1500

(continued)

Table 14.2 (continued)

Spec. title	References	Failure load (kN)	Modulus of elasticity (GPa)	FRP Type	Rft ratio	Cylindrical comp. strength (MPa)	Width of column (mm)	Length of column (mm)	Depth of slab (mm)	Width of slab (mm)	Length of slab (mm)
B-5		217	45.6	GFRP	0.42	33.5	150	150	130	1500	1500
B-6		222	45.6	GFRP	0.42	28.4	150	150	130	1500	1500
B-7		253	45.6	GFRP	0.42	46	150	150	130	1500	1500
G200n	Bouguerra et al. (2011)	732	43	GFRP	1.2	49.1	600	250	155	2500	3000
G175N		484	43	GFRP	1.2	35	600	250	135	2000	3000
G150N		362	43	GFRP	1.2	35	600	250	110	2000	3000
G175h		704	43	GFRP	1.2	65	600	250	135	2000	3000
G175n0.7		549	43	GFRP	0.7	53	600	250	135	2000	3000
G175n0.35		506	43	GFRP	0.35	53	600	250	137	2000	3000
C175N		530	122	GFRP	0.4	40.5	600	250	140	2000	3000
A	Zhu and Wang (2012) Nguyen-Minh and Rovnak (2013)	176	45.6	GFRP	0.42	22.5	150	150	130	1500	1500
B-2		209	45.6	GFRP	0.42	32.5	150	150	130	1500	1500
B-3		245	45.6	GFRP	0.55	32.5	150	150	130	1500	1500
B-4		167	45.6	GFRP	0.3	33	150	150	130	1500	1500
C		252	45.6	GFRP	0.42	44.5	150	150	130	1500	1500
GSL-PUNC-0.4		180	48	GFRP	0.48	49	200	200	130	2200	2200

(continued)

Table 14.2 (continued)

Spec. title	References	Failure load (kN)	Modulus of elasticity (GPa)	FRP Type	Rft ratio	Cylindrical comp. strength (MPa)	Width of column (mm)	Length of column (mm)	Depth of slab (mm)	Width of slab (mm)	Length of slab (mm)
GSL-PUNC-0.5		212	48	GFRP	0.68	49	200	200	130	2200	2200
GSL-PUNC-0.6		244	48	GFRP	0.92	49	200	200	130	2200	2200
G (0.7) 30/20	Hassan et al. (2017)	329	48.2	GFRP	0.7	34.5	300	300	135	2500	2500
G (1.6) 30/20		431	48.1	GFRP	1.55	38.5	300	300	130	2500	2500
G (1.6) 30/20-H		547	57.4	GFRP	1.55	76	300	300	130	2500	2500
G (1.2) 30/20		438	64.9	GFRP	1.2	37.5	300	300	130	2500	2500
G (0.3) 30/35		825	48.2	GFRP	0.35	34.5	300	300	285	2500	2500
G (0.7) 30/35		1071	48.1	GFRP	0.75	39.5	300	300	285	2500	2500
G (1.6) 30/35		1492	56.7	GFRP	1.6	38.5	300	300	275	2500	2500
G (1.6) 30/35-H		1600	56.7	GFRP	1.6	76	300	300	275	2500	2500
G (0.7) 30/20-B		386	48.2	GFRP	0.7	38.5	300	300	135	2500	2500
G (0.7) 45/20		400	48.2	GFRP	0.7	45	300	300	135	2500	2500
G (1.6) 45/20-B		511	48.1	GFRP	1.55	39.5	300	300	130	2500	2500
G (0.3) 30/35-B		781	48.2	GFRP	0.35	39.5	300	300	285	2500	2500
G (0.7) 30/35-B-2		1195	48.1	GFRP	0.75	46.5	300	300	280	2500	2500
G (0.3) 45/35		911	48.2	GFRP	0.35	48.5	300	300	285	2500	2500

(continued)

Table 14.2 (continued)

Spec. title	References	Failure load (kN)	Modulus of elasticity (GPa)	FRP Type	Rft ratio	Cylindrical comp. strength (MPa)	Width of column (mm)	Length of column (mm)	Depth of slab (mm)	Width of slab (mm)	Length of slab (mm)
G (1.6) 30/20-B		451	48.1	GFRP	1.55	32.5	300	300	130	2500	2500
G (1.6) 45/20		504	48.1	GFRP	1.55	32.5	300	300	130	2500	2500
G (0.7) 30/35-B-1		1027	48.1	GFRP	0.75	29.5	300	300	180	2500	2500
G(0.3) 45/35-B		1020	48.2	GFRP	0.35	32.5	300	300	285	2500	2500
G (0.7) 45/35		1248	48.1	GFRP	0.75	29.5	300	300	280	2500	2500
GSC-0.9-XX-0.4	El-Gendy and El-Salakawy (2015)	251	60.505	GFRP	0.9	41	300	300	160	1500	2800
GSC-1.35-XX-0.4		268	60.505	GFRP	1.35	41	300	300	160	1500	2800
GSC-1.8-XX-0.4		277	60.505	GFRP	1.7	41	300	300	160	1500	2800
GSC-0.9-XX-0.2		239	60.505	GFRP	0.85	41	300	300	160	1500	2800
GSC-0.9-XX-0.3		159	60.505	GFRP	0.9	41	300	300	160	1500	2800
GRD-0.9-XX-0.4		191	59.877	GFRP	0.9	41	300	300	160	1500	2800
G-0.6%-12-125T&B	Tharmarajah et al. (2015)	344	67.4	GFRP	0.6	68	500	25	120	500	1425
G-0.6%-16-300T&B		365	67.4	GFRP	0.6	65	500	25	117	500	1425
B-0.6%-12-125T&B		300	54	BFRP	0.6	69.5	500	25	120	500	1425
B-0.6%-16-300T&B		295	54	BFRP	0.6	66	500	25	117	500	1425

(continued)

Table 14.2 (continued)

Spec. title	References	Failure load (kN)	Modulus of elasticity (GPa)	FRP Type	Rft ratio	Cylindrical comp. strength (MPa)	Width of column (mm)	Length of column (mm)	Depth of slab (mm)	Width of slab (mm)	Length of slab (mm)
GSC-0.9-XX-0.4	Mostafa (2016)	251	60.505	GFRP	0.88	81	300	300	160	1450	2600
GSC-1.35-XX-0.5		272	60.505	GFRP	1.28	85	300	300	160	1450	2600
GSC-1.8-XX-0.4		288	60.505	GFRP	1.7	80	300	300	160	1450	2600
S2-B	Fareed et al. (2016)	548	69.3	BFRP	0.8	48.7	600	250	160	2000	3000
S3-B		665	69.3	BFRP	0.8	42.5	600	250	160	2000	3000
S4-B		566	69.3	BFRP	0.8	42.5	600	250	160	2000	3000
S5-B		716	69.3	BFRP	1.2	48	600	250	160	2000	3000
S6-B		576	69.3	BFRP	0.4	48	600	250	160	2000	3000
S7-B		436	69.3	BFRP	0.4	48	600	250	160	2000	3000
GN-0.65	Gouda and El-Salakawy (2016a)	363	69.3	GFRP	0.65	42	300	300	160	2600	2600
GN-0.98		378	68	GFRP	0.98	38	300	300	160	2600	2600
GN-1.30		425	68	GFRP	1.3	39	300	300	160	2600	2600
GH-0.65		380	68	GFRP	0.65	70	300	300	160	2600	2600
G-00-XX	Gouda and El-Salakawy (2016b)	421	68	GFRP	0.65	38	300	300	160	2800	2800
G-15-XX		363	68	GFRP	0.65	42	300	300	160	2800	2800
G-30-XX		296	68	GFRP	0.65	42	300	300	160	2800	2800
R-15-XX		320	68	GFRP	0.65	40	300	300	160	2800	2800

(continued)

Table 14.2 (continued)

Spec. title	References	Failure load (kN)	Modulus of elasticity (GPa)	FRP Type	Rft ratio	Cylindrical comp. strength (MPa)	Width of column (mm)	Length of column (mm)	Depth of slab (mm)	Width of slab (mm)	Length of slab (mm)
NW59	Oskouei et al. (2017)	719	68	GFRP	0.7	59	250	250	175	800	800
SG1	Abduljaleel et al. (2017)	136	47	GFRP	0.22	30	150	150	60	1100	1100
SO1		68	47	GFRP	0.13	37.5	150	150	60	1100	1100
SO2		85	47	GFRP	0.13	32.5	150	150	60	1100	1100
SO3		80	47	GFRP	0.22	30.5	150	150	60	1100	1100
SO4		100	47	GFRP	0.22	35.5	150	150	60	1100	1100
SO5		102	47	GFRP	0.22	30	150	150	60	1100	1100
GFS1	Ju et al. (2018)	410	47	GFRP	1.55	36.5	200	200	180	2200	3000
GFS2		360	47	GFRP	1.2	36.5	200	200	180	2200	3000
GFS3		370	47	GFRP	0.8	36.5	200	200	180	2200	3000
H-1.0-XX	Hussein and El-Salakawy (2018)	461	65	GFRP	0.98	80	300	300	160	2800	2800
H-1.5-XX		541	65	GFRP	1.45	84	300	300	160	2800	2800
H-2.0-XX		604	65	GFRP	1.93	87	300	300	160	2800	2800
C-F-S-10-4	Hemzah et al. (2019)	103	144	CFRP	0.3	51	100	100	80	600	600
C-F-S-10-6		127	144	CFRP	0.45	52	100	100	80	600	600
S-F-D-10-4		112	144	CFRP	0.6	46	100	100	80	600	600

(continued)

Table 14.2 (continued)

Spec. title	References	Failure load (kN)	Modulus of elasticity (GPa)	FRP Type	Rft ratio	Cylindrical comp. strength (MPa)	Width of column (mm)	Length of column (mm)	Depth of slab (mm)	Width of slab (mm)	Length of slab (mm)
S-F-D-10-6		129	144	CFRP	0.9	60	100	100	80	600	600
S-F-S-10-4		79	144	CFRP	0.3	52	100	100	80	600	600
S-F-S-10-6		107	144	CFRP	0.45	48	100	100	80	600	600
S-F-S-7.5-4		57	144	CFRP	0.4	49	100	100	60	600	600
S-F-S-7.5-6		79	144	CFRP	0.6	49	100	100	60	600	600
G	Salama et al. (2019)	314	65	GFRP	1.55	41.5	300	300	160	1350	2500
G1 (1.06)	Eladawy et al. (2019) Gu (2020)	140	62.6	GFRP	1.05	52.5	300	300	150	2500	2500
G2 (1.51)		140	62.6	GFRP	1.5	92.2	300	300	150	2500	2500
G3 (1.06)-SL		180	62.6	GFRP	1.05	45.2	300	300	150	2500	2500
A30-1		191	51.1	GFRP	1.28	27.5	300	300	90	1500	1500
A30-2		289	51.1	GFRP	1.05	27.5	300	300	110	1500	1500
A30-3		413	51.1	GFRP	0.82	26.5	300	300	140	1500	1500
A30-4		209	51.1	GFRP	1.31	27	350	350	85	1500	1500
A40-1		232	51.1	GFRP	1.28	28	350	350	85	1500	1500
A40-2		221	51.1	GFRP	0.88	26.5	350	350	85	1500	1500
A40-3		236	51.1	GFRP	1.28	28.5	300	300	85	1500	1500

(continued)

Table 14.2 (continued)

Spec. title	References	Failure load (kN)	Modulus of elasticity (GPa)	FRP Type	Rft ratio	Cylindrical comp. strength (MPa)	Width of column (mm)	Length of column (mm)	Depth of slab (mm)	Width of slab (mm)	Length of slab (mm)
A50-1		253	51.1	GFRP	1.28	29.5	300	300	85	1500	1500
A50-2		237	54.1	GFRP	0.88	32.5	300	300	85	1500	1500
A50-3		280	51.1	GFRP	1.28	26.5	350	350	85	1500	1500
S40-1	Zhou (2020)	314	51.1	GFRP	0.98	32.5	300	300	85	1500	1500
S50-1		187	54.4	GFRP	0.7	43.5	300	300	85	1500	1500
G4 (1.06)-H	Eladawy et al. (2020)	134	62.6	GFRP	1.05	92	300	300	150	2500	2500
F1	Huang et al. (2020)	262	123	CFRP	0.88	25	200	200	125	1600	1600
G-N-0.3	Salama et al. (2021)	260	65	GFRP	1.05	37	300	300	160	1300	2500
G-H-0.3		306	65	GFRP	1.05	86	200	200	160	2200	3000
G-N-0.6		178	65	GFRP	1.05	39	200	200	160	2200	3000
G-H-0.6		213	65	GFRP	1.05	86	200	200	160	2200	3000
0F-605	AlHamaydeh and Orabi (2021)	463	50.6	GFRP	2.8	38.5	250	250	125	2000	2000
0F-80F		486	50.6	GFRP	2.1	38.5	250	250	125	2000	2000
0F-1105		436	50.6	GFRP	1.55	38.5	250	250	125	2000	2000
1.25F-60S		455	50.6	GFRP	2.8	38.5	250	250	125	2000	2000
1.25F-80S		506	50.6	GFRP	2.1	38.5	250	250	125	2000	2000

(continued)

Table 14.2 (continued)

Spec. title	References	Failure load (kN)	Modulus of elasticity (GPa)	FRP Type	Rft ratio	Cylindrical comp. strength (MPa)	Width of column (mm)	Length of column (mm)	Depth of slab (mm)	Width of slab (mm)	Length of slab (mm)
1.25F-110S		498	50.6	GFRP	1.55	38.5	250	250	125	2000	2000
SA1	Mohmmad et al. (2022)	30	50	BFRP	0.85	45.2	55	55	35	500	500
SA2		28	42	GFRP	0.85	45.2	55	55	35	500	500
SA4		26	50	BFRP	0.55	45.2	55	55	35	500	500
SA5		24	42	GFRP	0.55	45.2	55	55	35	500	500
SA7		35	50	BFRP	0.85	45,2	55	55	35	500	500
SA0		28	50	BFRP	0.85	45.2	55	55	35	500	500
CFRP1	Shill et al. (2022)	169	140	CFRP	0.35	29.5	1075	1075	50	1670	1670
CFRP2		178	140	CFRP	0.35	34.5	1075	1075	50	1670	1670
CFRP3		208	140	CFRP	0.35	34.5	1075	1075	50	1670	1670
BFRP1		103	55	BFRP	0.35	29.5	1075	1075	50	1670	1670
BFRP2		120	55	BFRP	0.35	34.5	1075	1075	50	1670	1670
BFRP3		144	55	BFRP	0.35	34.5	1075	1075	50	1670	1670
Minimum		24.34	28.4		0.13	22.2	25	25	35	300	300
Maximum		1600	230		3.75	179	1075	1075	285	4000	3000
Mean		372	75		1	44	303	235	125	1715	1915
Variation		82%	55%		65%	45%	65%	65%	39%	39%	40%

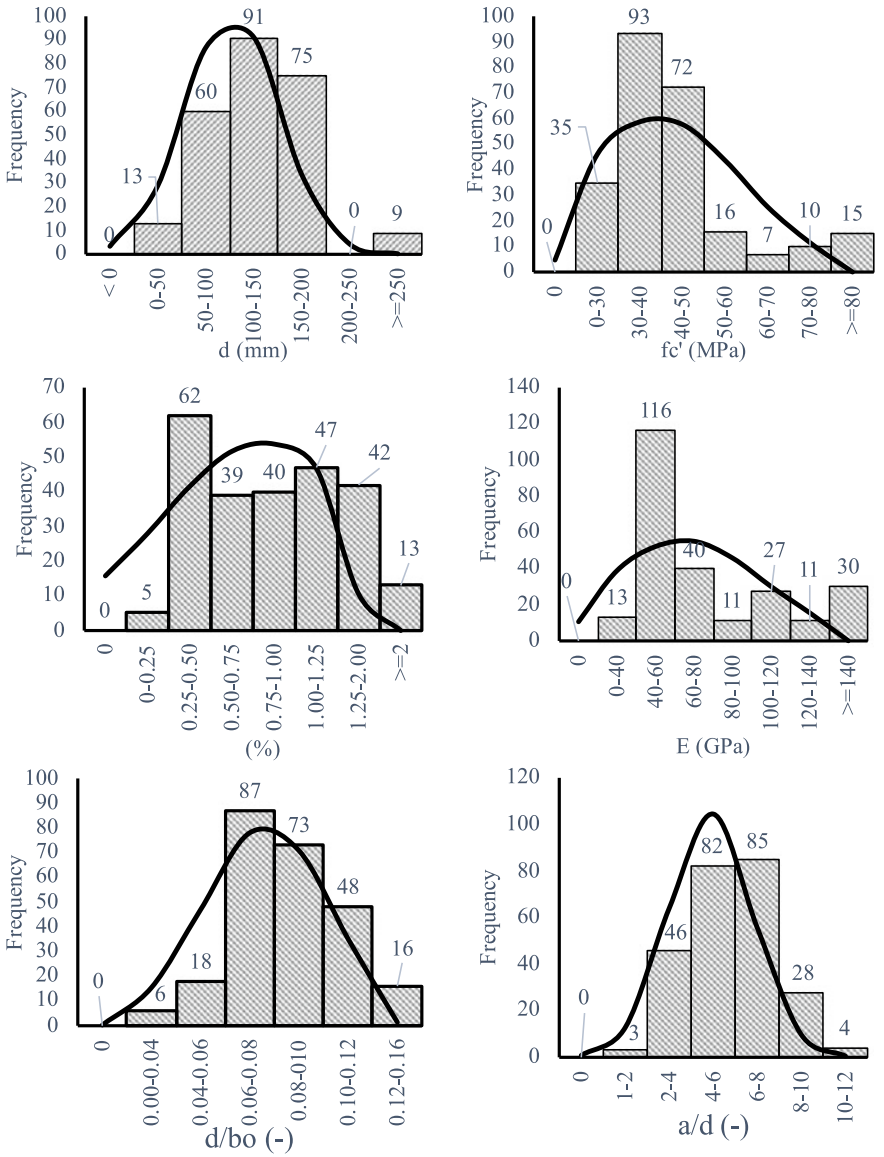

Fig. 14.2 The tested column-slab connections' frequencies and ranges when using FRP

value greater than unity implies a conservative estimate. If the SR value is less than 1.0, the prediction is cautious, and the shear strength was underestimated.

As indicated in Table 14.2 and Fig. 14.3, lower values with a 95% accuracy level (lower 95%), maximum values, and minimum–maximum values were applied to the SR for each model that was chosen. For furthering the development of the design

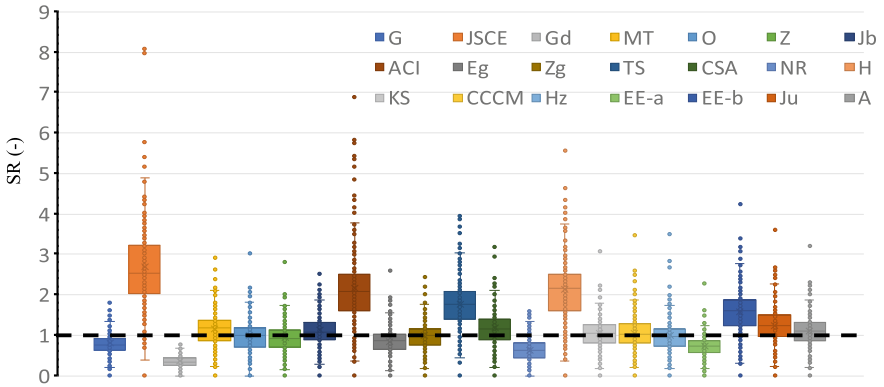

Fig. 14.3 The effectiveness of chosen models

models, Table 14.2 displays the statistical goodness and central tendency of fit of all chosen models. With an average value of 2.71, 2.16, and 2.18 respectively, the JSCE, H models, and ACI, are overly cautious. In comparison to other models with coefficients of variation of 35%, 35%, 36%, and 36%, respectively, the models, and Zg, EE-b, Ju are more consistent.

For each of the chosen models, a box plot is shown in Fig. 14.2. Extreme values and a wide range are shown in the ACI. Furthermore, when the GD and NR were used, extremely un-conservative predictions were produced. The strength (Mean near to 1.0) is accurately predicted by the current models (i.e., Ju, EE-a, Hz, and A) as illustrated in Fig. 14.3. As indicated in Table 14.3, the consistency is still deficient (i.e., C.O.V. is higher than 35.0%). In comparison to mechanically based models (CCCM) and fracture-based models, models that consider fundamental factors in a power form equation appear the most exact and consistent (NR). Furthermore, it is evident from Fig. 14.3 that each technique was created or calibrated with a nonsystematic margin of safety determined by the discretion and expertise of each develop. d NR. An evaluation of dependability that takes resistance and load uncertainty into account should be used to control this. Although it is a fascinating issue, it is outside the purview of this study and may be explored further. Further enhanced mechanically based models that make physical sense and are easy to construct are also required.

14.4.1 Effective Depth

Figure 14.4 plots the computed SR value against the effective depth using the American code model, the CSA model, the Ju model, the JSCE model, the model of CCCM, and the model of EE-B. Additionally, the slopes of the best fit line were presented for the JSCE model, the ACI model, the CSA model, the CCCM model, the EE-B model, and the Ju model, respectively. These slopes were 0.0011, 0.003, 0.0016,

Table 14.3 For all strength in models, statistical measurements

Model designed	Determination coefficients mean	Error of mean square root	Mean error	C.O.V	Average	Min	Max	Lower 95%
G	0.66	205	143	0.37	0.81	0.15	1.85	0.78
JSCE	0.69	335	237	0.38	2.7	0.69	8.07	2.58
Gd	0.7	775	653	0.37	0.35	0.08	0.78	0.35
MT	0.68	182	120	0.36	1.18	0.24	2.93	1.12
O	0.71	171	110	0.38	1	0.17	3.02	0.94
Z	0.68	201	125	0.38	0.95	0.16	2.8	0.91
Jb	0.66	181	110	0.38	1.15	0.2	2.6	1.1
ACI	0.69	273	194	0.45	2.18	0.37	6.9	2.05
Eg	0.68	222	136	0.36	0.85	0.14	2.6	0.83
Zg	0.71	166	105	0.35	1	0.18	2.44	0.95
TS	0.7	255	175	0.35	1.78	0.34	3.95	1.7
CSA	0.72	165	111	0.4	1.2	0.2	3.18	1.15
NR	0.55	360	253	0.45	0.64	0.15	1.6	0.6
H	0.7	291	205	0.36	2.16	0.4	5.55	2.08
KS	0.72	165	104	0.38	1.06	0.18	3.06	1.03
CCCM	0.66	198	127	0.44	1.06	0.22	3.47	1
Hz	0.73	166	105	0.45	1	0.19	3.55	0.95
EE-a	0.66	302	195	0.37	0.75	0.12	2.27	0.7
EE-b	0.71	232	160	0.35	1.6	0.3	4.25	1.55
Ju	0.7	173	118	0.35	1.25	0.22	3.6	1.2
A	0.71	164	105	0.36	1.15	0.2	3.2	1.08

0.0019, 0.0003, and 0.0025. Except for the JSCE, the safety of the chosen models declines as depth increases. The SR value that was determined using the EE-B model has the lowest best fit line, making it the most consistent regarding depth. The ACI model, however, produced the greatest SR value, making it the least consistent. This could be because the American code model doesn't account for size effects.

14.4.2 Concrete Compression Strength

Figure 14.5 compares the computed SR value to the concrete compressive strength using the American code model, the CSA model, the JSCE model, the Ju model, the CCCM model, and the EE-B model. The best fit line was also displayed, and its slopes for the JSCE model, the CSA model, the ACI model, the EE-B model, the

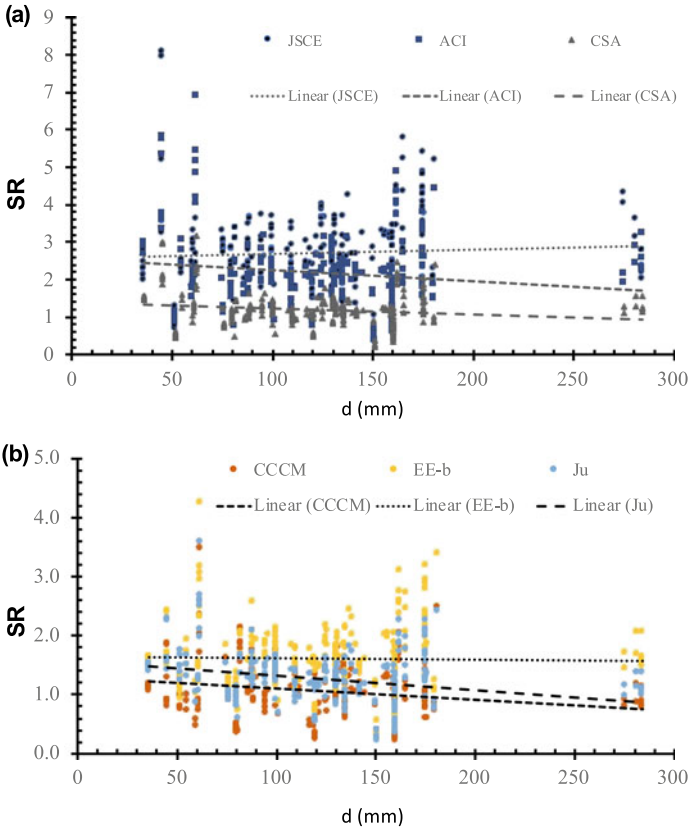

Fig. 14.4 The impact of depth on the SR value

CCCM model, and the Ju model, respectively, were 0.0019, 0.0174, 0.0046, 0.0017, 0.0031, and 0.0027. The CCCM model, the EE-B model, and the Ju model are less safe as concrete compressive strength increases. On the other hand, if compressive strength of concrete grows, the safety of the JSCE, ACI, and CSA models also does. It is most consistent with the concrete compressive strength since the more fit line for the SR value that was determined using the EE-b model is the lowest. Though it is the least reliable, employing the CSA model produced the greatest SR value.

14.4.3 Ratio of Flexure Reinforcement

In comparison to the flexure reinforcement ratio, Fig. 14.6 displays the value of SR estimated using the Ju model, American code model, the CSA model, the JSCE model, the CCCM model, and the EE-B model. The best fit line was also displayed,

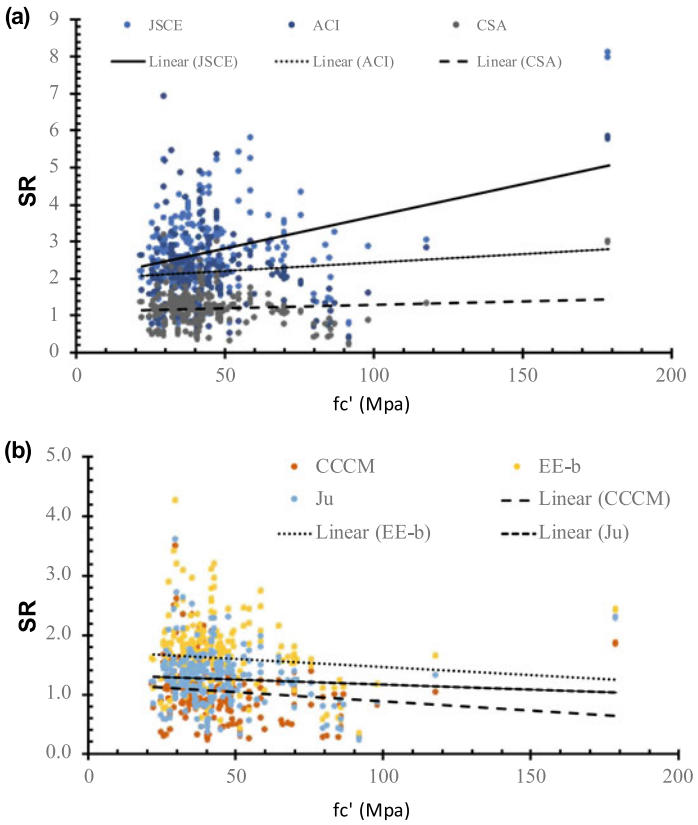

Fig. 14.5 The impact in compressive strength of concrete on the value of SR

and its slopes for the JSCE model, the ACI model, the CSA model, the Ju model, the EE-B model, and the CCCM model, respectively, were 0.2529, 0.6244, 0.1844, 0.0328, 0.1817, and 0.2229. Except for the JSCE model, the safety of the chosen models declines as the flexural reinforcement ratio increases. It is most consistent with the flexure reinforcement ratio that the more fit line for the SR value that was determined using the CCCM model is the lowest. The least consistent model, however, is the one that used the American code model since it produced the greatest value of SR. This may be because of the American code model leaving out the flexure reinforcement ratio.

14.4.4 Young's Modulus

In contrast to the Young's modulus, Fig. 14.7 displays the value of SR estimated using the EE-B model, the American code model, the JSCE model, the CCCM

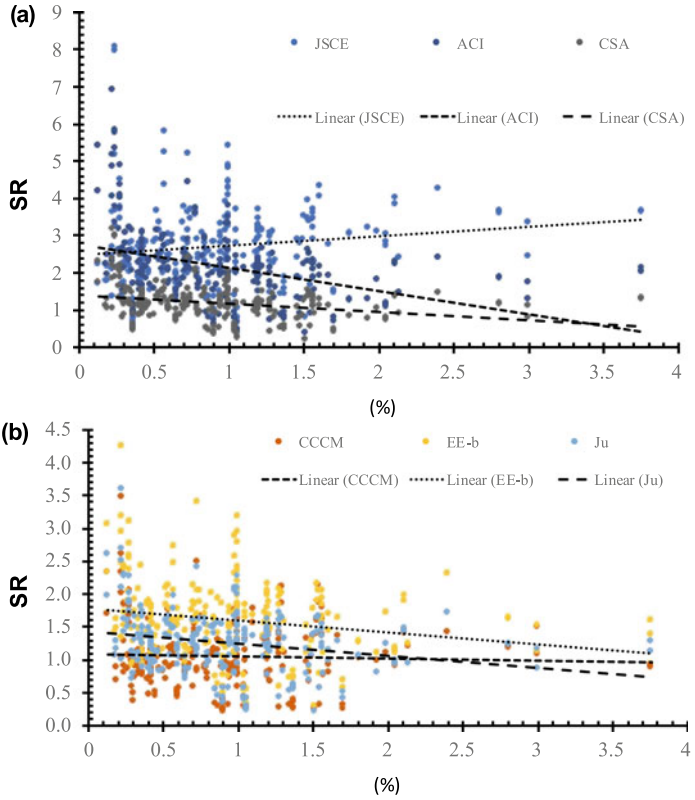

Fig. 14.6 The impact of the reinforcement in flexural ratio on the value of SR

model, the CSA model, and Ju model them. Additionally, the slopes of the best fit line were presented for the JSCE model, the American code model, the CSA model, the CCCM model, the EE-B model, and the Ju model, respectively. Slopes 0.0002, 0.0012, 0.0013, 0.002, 0.0011, and 0.0075were used. Except for the EE-b model and the CCCM model, the safety of chosen models rises as Young's modulus increases. The value of SR that was estimated using the Ju model has the lowest best fit line, making it the Young's modulus most consistently constant. The least consistent model was the one that used the JSCE model since it produced the greatest SR value.

14.4.5 Ratio of Depth to Control Perimeter

The SR value estimated using the American code model, the CCCM model, the CSA model, the JSCE model, the Ju model, and the EE-B model is displayed in Fig. 14.8

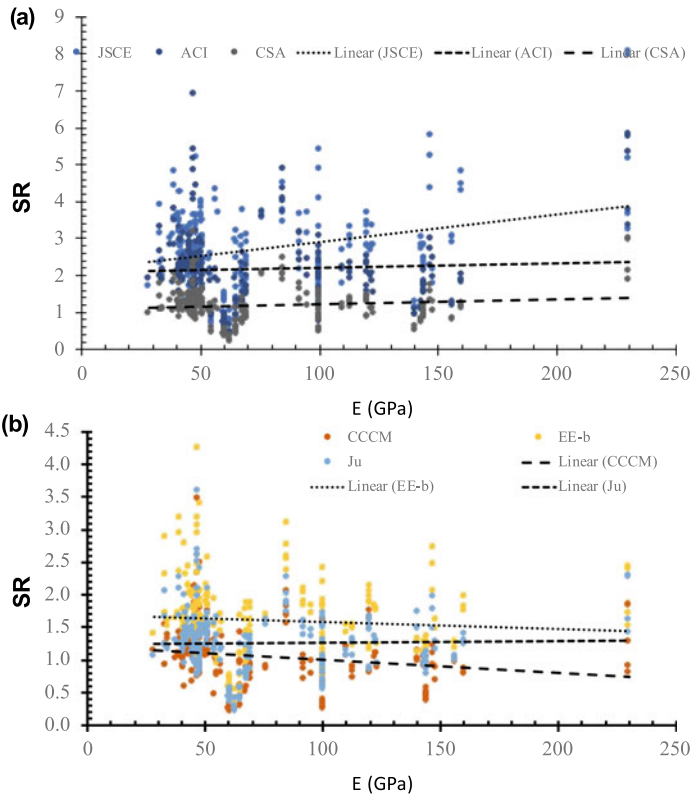

Fig. 14.7 The Young's modulus' impact on the value of SR

in comparison to the depth-to-control perimeter ratio. For the JSCE model, the ACI model, the CSA model, the CCCM model, the EE-B model, and the Ju model, the best fit line was also drawn. Its slope was 8.5935, 2.4433, 6.8699, 13.86, 0.8117, and 1.6327, respectively. As the depth-to-control perimeter ratio rises, the safety of the EE-b model, the CCCM model, and the Ju model also declines. However, when the ratio of depth to control perimeter grows, the safety of the ACI, JSCE, and CSA models also rises. It is most consistent with the depth to control perimeter ratio since the more fit line for the value of SR that was derived using the EE-b model is the lowest and is as a result. The American code model, however, produced the greatest SR value, making it the least consistent. The American code model might not have taken this parameter's influence into account, for whatever reason.

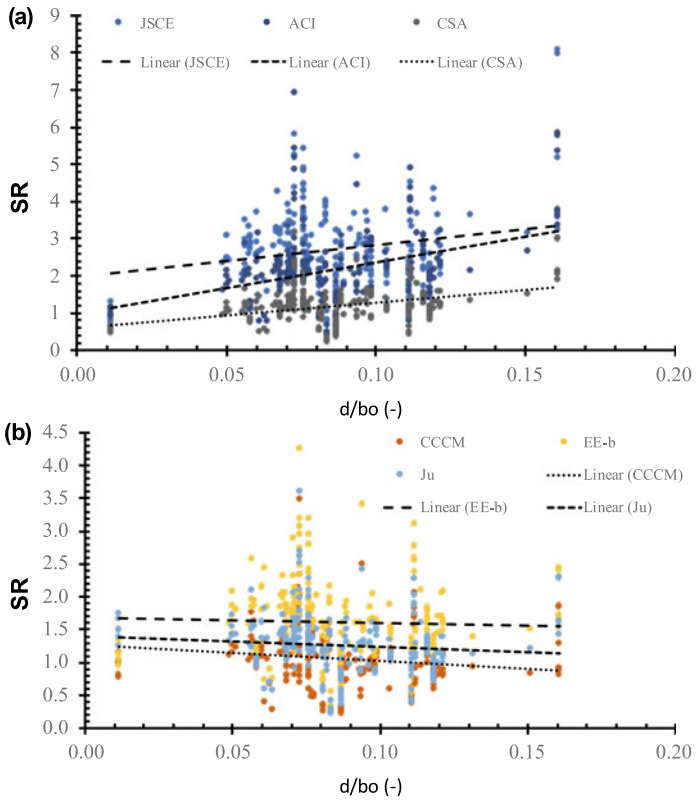

Fig. 14.8 The impact of the between depth and control perimeter on the value of SR

14.4.6 Span-to-Depth Ratio for Shear

Figure 14.9 compares the computed the value of SR to the shear span-to-effective depth ratio using the American code model, the JSCE model, the CSA model, the EE-B model, the Ju model, and the CCCM model. The slope of the best fit line, which was plotted separately for the JSCE model, the American code model, the CSA model, the CCCM model, the EE-b model, and the Ju model, was 0.0507, 0.0475, 0.0224, 0.0213, 0.023, and 0.1353. With an increase in the shear span-to-effective depth ratio, the safety of the JSCE model, the ACI model, and the CSA model declines. On the other hand, when the ratio of shear span to effective depth rises, the safety of the CCCM model, the EE-b model, and the Ju model also rises. They are the most consistent regarding the shear span-to-effective depth ratio since the CSA model, the Ju model, and the EE-b model have the lowest best fit line for the SR value. However, the CCCM model produced the greatest results; hence, it is the least consistent.

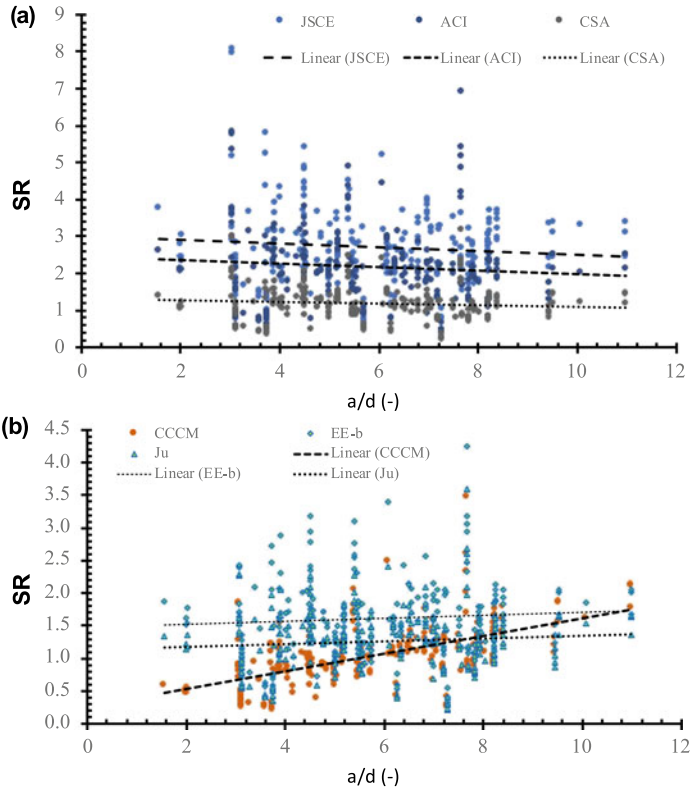

Fig. 14.9 The impact of the shear depth-to-span ratio on the value of SR is determined

14.5 Future Research

Future research studies might focus on a number of these areas, which were noted: (1) A reliability-based examination of the design's safety that takes into account the loads' variability as well as that of the geometry, the materials, and the constructions; (2) A simple-to-design mechanical model that is more dependable and consistent and makes sense in terms of physics.

14.6 Conclusions

Twenty-one concrete slabs chosen approaches for expected punching shear strength were evaluated for accuracy. Comparisons between forecasts and measured strengths from a large experimental database, including 248 slabs from more than 50 research

papers, were used to examine for the method's capacity to predict the two way strength in un-reinforcement concrete slabs in shear.

1. In terms of the effect of size, concrete compressive strength, depth to control perimeter ratio, and shear span-to-depth ratio, the EE-B model exhibits the greatest consistency. This is because it is based on the mechanical principles and uses empirically observed behavior.
2. A number of statistical techniques were used, and the impact of the different fundamental factors was explored. Because of this, the JSCE, ACI, and H models, which have average values of 2.71, 2.18, and 2.16, respectively, are too cautious. In comparison to other models, where the variational coefficients are 35%, 35%, 36%, and 36%, respectively, the Ju, Zg, EE-b, and A models are more consistent.

References

A. C. I. ACI-440 (2015) Guide for the design and construction of concrete reinforced with FRP bars (ACI 440.1R-15). ACI, Farmington Hills, Michigan, USA

Abduljaleel MT, Mahmoud AS, Yousif A (2017) Experimental investigation of two-way concrete slabs with openings reinforced with glass fiber reinforced polymer bars. J Eng Sci Technol 12:889–912

Ahmad HS, Zia P, Yu TJ, Xie Y (1993) Punching shear tests of slabs reinforced with 3-dimensional carbon fiber fabric. Concr Int 16:36–41

AlHamaydeh M, Orabi MA (2021) Punching shear behavior of synthetic fiber-reinforced self-consolidating concrete flat slabs with GFRP bars. J Compos Constr 25:04021029

Ali AH, Mohamed HM, Chalioris CE, Deifalla A (2021) Evaluation of the shear design equations of FRP-reinforced concrete beams without shear reinforcement. Eng Struct 235. Elsevier

Alrudaini TMS (2022) A rational formula to predict punching shear capacity at interior columns connections with RC flat slabs reinforced with either steel or FRP bars but without shear reinforcement. Structures 37:56–68

Bank L, Xi Z (1995) Punching shear behavior of pultruded FRP grating reinforced concrete slabs. In: Proceedings of the non-metallic (FRP) reinforcement for concrete structures. CRC Press, Boca Raton, FL, USA, pp 360–367

Banthia N, Al-Asaly M, Ma S (1995) Behavior of concrete slabs reinforced with fiber-reinforced plastic grid. ASCE J Mater Civ Eng 7:252–257

Bouguerra K, Ahmed EA, El-Gamal S, Benmokrane B (2011) Testing of full-scale concrete bridge deck slabs reinforced with fiber-reinforced polymer (FRP) bars. Constr Build Mater 25:3956–3965

Bywalski C, Drzazga M, Kamiński M, Kaźmierowski M (2020) A new proposal for the shear strength prediction of beams longitudinally reinforced with fiber-reinforced polymer bars. Buildings 10(5):86. https://doi.org/10.3390/buildings10050086

Collins MP (2001) Evaluation of shear design procedures for concrete structures. A CSA Technical Committee Reinforced Concrete Design Report by the Canadian Standards Association, Canada

CAN/CSA S806-12 (2012) Design and construction of building structures with fiber reinforced polymers (CAN/CSA S806-12). Canadian Standards Association: Rexdale, ON, Canada

Deifalla A (2015) Torsional behavior of rectangular and flanged concrete beams with FRP. J Struct Eng. ASCE. https://doi.org/10.1061/(ASCE)ST.1943-541X.0001322

Deifalla A (2020) Strength and ductility of lightweight reinforced concrete slabs under punching shear. Structures 27:2329–2345. https://doi.org/10.1016/j.istruc.2020.08.002

Deifalla A (Mar 2021a) A mechanical model for concrete slabs subjected to combined punching shear and in-plane tensile forces. Eng Struct 231. Elsevier
Deifalla A (2021b) A strength and deformation model for prestressed lightweight concrete slabs under punching shear. Adv Struct Eng 1–12. https://doi.org/10.1177/13694332211020408
Deifalla A (2022) Punching shear strength and deformation for FRP-reinforced concrete slabs without shear reinforcement. Case Stud Constr Mater 16:e00925. p. j. cscm. e00925
Deifalla AF, Zapris AG, Chalioris CE (2021) Multivariable regression strength model for steel fiber-reinforced concrete beams under torsion. Materials 14:3889. https://doi.org/10.3390/ma14143889
Deifalla A, Khali MS, Abdelrahman A (2015) Simplified model for the torsional strength of concrete beams with GFRP stirrups. Compos Constr, ASCE 19(1):04014032. https://doi.org/10.1061/(ASCE)CC.1943-5614.0000498
Deifalla A, Hamed M, Saleh A, Ali T (2014) Exploring GFRP bars as reinforcement for rectangular and L-shaped beams subjected to significant torsion: an experimental study. Eng Struct 59:776–786
Ebid A, Deifalla A (2021) Prediction of shear strength of FRP reinforced beams with and without stirrups using (GP) technique. Ain Shams Eng J. Elsevier. https://doi.org/10.1016/j.asej.2021.02.006
Eladawy B, Hassan M, Benmokrane B (2019) Experimental study of interior glass fiber-reinforced polymer-reinforced concrete slab-column connections under lateral cyclic load. ACI Struct J 116:165–180
Eladawy M, Hassan M, Benmokrane B, Ferrier E (2020) Lateral cyclic behavior of interior two-way concrete slab–column connections reinforced with GFRP bars. Eng Struct 209:109978
El-Gamal S, El-Salakawy E, Benmokrane B (2005) Behaviour of concrete bridge deck slabs reinforced with fiber-reinforced polymer bars under concentrated loads. ACI Struct J 102(5):727–735
El-Gamal S, El-Salakawy E, Benmokrane B (2007) Influence of reinforcement on the behaviour of concrete bridge deck slabs reinforced with FRP bars. J Compos Constr ASCE 11:449–458
El-Gendy MGS, El-Salakawy EF (2020) Assessment of punching shear design models for FRP-RC slab–column connections. J Compos Constr 24:04020047. https://doi.org/10.1061/(ASCE)CC.1943-5614.0001054
El-Gendy M, El-Salakawy E (2015) Punching shear behaviour of GFRP-RC edge slab-column connections. In: Proceedings of the 7th international conference on FRP composites in civil engineering, pp 1–6
El-Ghandour AW, Pilakoutas K, Waldron P (2003) Punching shear behavior of fiber reinforced polymers reinforced concrete flat slabs: experimental study. J Compos Constr 7(2003):258–265
Elmeligy O, El-Nemr A, Deifalla A (2017) Reevaluating the modified shear provision of CAN/CSA S806-12 for concrete beams reinforced with FRP stirrups. In: AEI Conference, ASCE, Oklahoma City
Zhang Q (2006) Behavior of two-way slabs reinforced with CFRP bars. A thesis submitted to the school of graduate studies in partial fulfillment of the requirement for the degree of Master Engineering, Faculty of engineering and Applied Science, Memorial University of Newfoundland, New Found land, Canada
Deifalla A (2021) Refining the torsion design of fibered concrete beams reinforced with FRP using multi-variable non-linear regression analysis for experimental results. Eng Struct 224. Elsevier
Fareed E, Ahmed EA, Benmokrane B (2016) Experimental testing WMCAUS IOP conference series: materials science and engineering; IOP Publishing, Bristol, UK, p 032064. https://doi.org/10.1088/1757-899X/245/3/032064
FIB (2007) FRP reinforcement in RC structures, Technical report prepared by a working party of Task Group 9.3: Fib Bulletin 40
Gardner NJ (1990) Relationship of the punching shear capacity of reinforced concrete slabs with concrete strength. ACI Struct J 87(1):66–71

Gouda A, El-Salakawy E (2016a) Behavior of GFRP-RC Interior Slab-Column Connections with Shear Studs and High-Moment Transfer. J Compos Constr 20:04016005. https://doi.org/10.1061/(ASCE)CC.1943-5614.0000663

Gouda A, El-Salakawy E (2016b) Punching shear strength of GFRPRC interior slab-column connections subjected to moment transfer. J Compos Constr ASCE 20:04015037. https://doi.org/10.1061/(ASCE)CC.1943-5614.0000597

Gu S (2020) Study on the punching shear behavior of FRP reinforced concrete slabs subjected to concentric loading. Master's thesis, Zhejiang University of Technology, Zhejiang, China

Hassan T, Abdelrahman A, Tadros G, Rizkalla S (2000) Fibre reinforced polymer reinforcing bars for bridge decks. Can J Civ Eng 27:839–849. https://doi.org/10.1139/l99-098

Hassan MM, Deifalla A (2015) Evaluating the new CAN/CSA-S806-12 torsion provisions for concrete beams with FRP reinforcements. Mater Struct. https://doi.org/10.1617/s11527-015-0680-9

Hassan M, Fam A, Benmokrane B (2017) A new punching shear design formula for frp-reinforced interior slab-column connections. In: Proceedings of the 7th international conference on advanced composite materials in bridges and structures, Vancouver, BC, Canada

Hemzah SA, Al-Obaidi S, Salim T (2019) Punching shear model for normal and high-strength concrete slabs reinforced with CFRP or steel bars. Jordan J Civ Eng 13:250–268

Huang Z, Zhao Y, Zhang J, Wu Y (2020) Punching shear behavior of concrete slabs reinforced with CFRP grids. Structures 26:617–625

Hussein AF, El-Salakawy E (2018) Punching shear behavior of glass fiber-reinforced polymer-reinforced concrete slab-column interior connections. ACI Struct J 115:1075–1088. https://doi.org/10.14359/51702134

Hussein A, Rashid I, Benmokrane B (2004) Two-way concrete slabs reinforced with GFRP bars. In: Proceedings of the 4th international conference on advanced composite materials in bridges and structures, CSCE, Calgary, AB, Canada

Jacobson DA, Bank LC, Oliva MG, Russel JS (2005) Punching shear capacity of double layer FRP grid reinforced slabs. ACI, Specs. Publication. SP. 230–49, pp 857–876

JSCE (1997) Recommendation for design and construction of concrete structures using continuous fiber reinforcing materials. Machida A (ed). Concrete Engineering Series 23, Tokyo, Japan, pp 325

Ju M, Park K, Park AC (2018) Punching shear behavior of two-way concrete slabs reinforced with glass-fiber-reinforced polymer (GFRP) bars. Polymers 10:893. https://doi.org/10.3390/polym10080893

Ju M, Ju J, Sim JW (2021) A new formula of punching shear strength for fiber reinforced polymer (FRP) or steel reinforced two-way concrete slabs. Compos Struct 258:113471. https://doi.org/10.1016/j.compstruct.2020.113471

Kara IF, Sinani B (2017) Prediction of punching shear capacity of two-ways FRP reinforced concrete slabs. Int J Bus Technol 5:57–63

Khanna O, Mufti A, Bakht B (2000) Experimental investigation of the role of reinforcement in the strength of concrete deck slabs. Can J Civil Eng 27:475–480

Kuchma D, Wei S, Sanders D, Belarbi A, Novak L (2019) The development of the one-way shear design provisions of ACI 318-19. ACI Struct J 116(4)

Lee JH, Yoon YS, Cook WD, Mitchell D (2009) Improving punching shear behavior of glass fiber-reinforced polymer reinforced slabs. ACI Struct J 106:427–434

Louka HJ (1999) Punching behavior of a hybrid reinforced concrete bridge deck. Master's thesis, University of Manitoba, Winnipeg, MB, Canada

Marí A, Bairán J, Cladera A, Oller E, Ribas C (2015) Shear-flexural strength mechanical model for the design and assessment of reinforced concrete beams. Struct Infrastruct Eng 11:1399–1419

Matthys S, Taerwe L (2000) Concrete slabs reinforced with FRP grids. II: punching resistance. J Compos Constr ASCE 4(3):154–161

Min KH, Yang JM, Yoo DY, Yoon YS (27–29 Sep 2010) Flexural and punching performances of FRP and fiber reinforced concrete on impact loading. In: Proceedings of the CICE 2010–the 5th international conference on FRP composites in civil engineering, Beijing, China

Mohmmad SH, Gülsan ME, Çevik A (2022) Punching shear behaviour of geopolymer concrete two-way slabs reinforced by FRP bars under monotonic and cyclic loadings. Adv Struct Eng 25:453–472

Mostafa A (2016) Punching shear behavior of GFRP-RC slab-column edge connections with high strength concrete and shear reinforcement. Master's thesis, Manitoba University, Winnipeg, MB, Canada, p 51

Nguyen-Minh L, Rovnak M (2013) Punching-shear resistance of interior GFRP reinforced slab-column connection. ASCE J Compos Constr 17:2–13

Oller E, Kotynia R, Marí A (2018) Assessment of the existing formulations to evaluate shear-punching strength in RC slabs with FRP bars without transverse reinforcement. In: High tech concrete: where technology and engineering meet; Springer, Cham, Switzerland. https://doi.org/10.1007/978-3-319-59471-2_91

Oskouei AV, Kivi MP, Araghi H, Bazli M (2017) Experimental study of the punching behavior of GFRP reinforced lightweight concrete footing. Mater Struct 50:256. https://doi.org/10.1617/s11527-017-1127-2

Ospina CE, Alexander SDB, Cheng JJR (2003) Punching of two- way slabs with fiber-reinforced polymer reinforcing bars or grids. ACI Struct J 100(2003):589–598

Rahman AH, Kingsley CY, Kobayashi K (2000) Service and ultimate load behavior of bridge deck reinforced with carbon FRP grid. J Compos Constr 4:16–23

Salama AE, Hassan M, Benmokrane AB (2019) Effectiveness of glass fiber-reinforced polymer stirrups as shear reinforcement in glass fiber-reinforced polymer-reinforced concrete edge slab-column connections. ACI Struct J 116:165–180

Salama AE, Hassan M, Benmokrane B (2021) Punching-shear behavior of glass fiber-reinforced polymer-reinforced concrete edge column-slab connections: experimental and analytical investigations. ACI Struct J 118:147–160

Shen Y, Sun J, Liang S (2022) Interpretable machine learning models for punching shear strength estimation of FRP reinforced concrete slabs. Crystals 12:259. https://doi.org/10.3390/cryst12020259

Shill S, Garcez E, Al-Ameri R, Subhani M (2022) Performance of two-way concrete slabs reinforced with basalt and carbon FRP rebars. J Compos Sci 6:74

Tharmarajah G, Taylor ES, Cleland J., Robinso D (2015) Corrosion-resistant FRP reinforcement for bridge deck slabs. In: Proceedings of the institution of civil engineers. Bridge Engineering; ICE Publishing, London, UK, vol 168, pp 208–217. https://doi.org/10.1680/jbren.13.00001

Theodorakopoulos DD, Swamy RN (2007) Analytical model to predict punching shear strength of FRP-reinforced concrete flat slabs. ACI Struct J 104:257–266

Tom EE (2007) Behavior of two-way slabs reinforced with GFRP bars. Master's thesis, Memorial University of Newfoundland, St. John's, NF, Canada, p 169

Wu L, Huang T, Tong Y, Liang S (2022) A modified compression field theory based analytical model of RC slab-column joint without punching shear reinforcement. Buildings 12:226. https://doi.org/10.3390/buildings12020226

Xiao Z (2010) Expremental study on two-way concrete slab subjected to punching shear. Master's thesis, Zhengzhou University, Zhengzhou, China

Yooprasertchai E, Dithaem R, Arnamwong T, Sahamitmongkol R, Jadekittichoke J, Joyklad P, Hussain Q (2021ab) Remediation of punching shear failure using glass fiber reinforced polymer (GFRP) rods. Polymers 13:2369. https://doi.org/10.3390/polym13142369

Yooprasertchai E, Tiawilai Y, Wittayawanitchai T, Angsumalee J, Joyklad P, Hussain Q (2021b) Effect of shape, number, and location of openings on punching shear capacity of flat slabs. Buildings 11:484. https://doi.org/10.3390/buildings11100

Zaghloul A (2007) Punching shear strength of interior and edge column slab connections in CFRP rein-forced flat plate structures transferring shear and moment. Ph.D. thesis, Department of Civil and Environmental Engineering, Carleton University, Ottawa, ON, Canada

Zaghloul A, Razaqpur A (2003) Punching shear behavior of CFRP reinforced concrete flat plates. In: Proceedings of the international conference on, composites in construction, pp 1–726

Zaghloul E, Mahmoud Z, Salama T (2008) Punching behavior and strength of two-way concrete slabs reinforced with glass fiber reinforced polymer (GFRP) rebars. In: Proceedings of structural composites for infrastructure applications, Hurghada, Egypt

Zhang Q (2006) Behaviour of two-way slabs reinforced with CFRP bars. Master's thesis, Memorial University of Newfoundland, St. John's, NF, Canada

Zhang Q, Marzouk H, Hussein A (2005) A preliminary study of high-strength concrete two-way slabs reinforced with GFRP bars. In: Proceedings of the 33rd CSCE annual conference: general conference and international history symposium, CSCE, Toronto, ON, Canada

Zhou X (2020) Expremental study on the punching shear behavior of square GFRP reinforced concrete slabs. Master's thesis, Zhejiang University of Technology, Zhejiang, China

Zhu HY, Wang JL (2012) Plastic analysis on punching shear capacity of two-way BFRP rebar reinforced concrete slabs under central concentrated load. J Zhengzhou Univ (Eng Sci) 33:1–5. (in Chinese)

Zhu H, Zhang Y, Gao D, Xiao Z (27–29 Sep 2010) Deformation behavior of concrete two-way slabs reinforced with BFRP bars subjected to eccentric loading. In: Proceedings of the CICE 2010: the 5th international conference on FRP composites in civil engineering, Beijing, China